Journal of Physics D: Applied Physics

**PAPER**

# Manipulation of the multiple bound states in the continuum and slow light effect in the all-dielectric metasurface

IOP Publishing

Journal of Physics D: Applied Physics

J. Phys. D: Appl. Phys. **56** (2023) 405109 (9pp)

https://doi.org/10.1088/1361-6463/acdf6a

# Manipulation of the multiple bound states in the continuum and slow light effect in the all-dielectric metasurface

**Suxia Xie[1,*], Siyi Sun[1], Zhijian Li[2,3,*], Jingcheng Yang[1], Weiwei Shen[1] and Xin Guan[1]**

[1] School of Mechanical Engineering, University of Shanghai for Science and Technology, Shanghai 200093, People's Republic of China

[2] College of Engineering Science and Technology, Shanghai Ocean University, Shanghai 201306, People's Republic of China

[3] National Engineering Laboratory for Robot Visual Perception and Control Technology, Hunan University, Changsha 410082, People's Republic of China

E-mail: xsx@usst.edu.cn and zj-li@shou.edu.cn

Received 20 April 2023, revised 7 June 2023

Accepted for publication 19 June 2023

Published 11 July 2023

**Abstract**

All-dielectric metasurface with ultra-high quality resonances underpinned by bound states in the continuum (BICs) have attracted lots of attention in recent years for they enable new methods of wavefront control and light focusing. We study a metasurface composed of one transverse nanohole (TNs) and two identical vertical nanoholes (VNs) in one lattice, which supports both symmetry-protected and accidental BICs (at-Γ and off-Γ BICs). Based on the destructive interference between the surface states from the TN element and the identical VNs element, two at-Γ BICs emerge, and they turn into quasi-BICs by rotating the electric field polarization direction of the incident plane wave from x to y. The off-Γ BICs come from destructive interference from different radiation channels, which are influenced by the in-plane structural parameters symmetry insignificantly. Two at-Γ BICs and one off-Γ BIC of the metasurface all have ultra-high Q-factors (exceeding $10^6$, $10^4$, and $10^6$, respectively), which means much in the application of biosensors. Especially, this nanostructure has outstanding ultra-slow light properties at BICs, with a group index about $10^6$, which underpin a new generation of flat-optics slow light devices.

Keywords: bound states in the continuum, metasurface, slow light, Q-factor, photonics crystal

(Some figures may appear in colour only in the online journal)

## 1. Introduction

Bound states in the continuum (BICs) with ultra-high quality factor (Q-factor) have gained rapid development in nanostructure [1]. They are associated with the decoupling of the resonant mode from the radiative spectrum of the surrounding space [1–4], which is first discovered in quantum mechanics [5]. Benefiting from the high-Q resonances of quasi-BICs, the metasurface can be designed to realize ultra-sharp transmittance/reflectance spectra with an ultra-high light–matter interaction strength [4, 6, 7]. Thus, BIC-based lasing [8, 9], beam shifting [10, 11], strong coupling [12, 13], modulation [14, 15], imaging [16] and sensing [17] have all then been successfully achieved. BICs in optics due to their broad potential applications in communications [18, 19], lasing [20–23], filtering [24–26], and sensing [27–29]. Resonant modes inside the continuum with finite lifetimes that lie within the light cone and consequently can couple to the extended waves and leak out with a complex frequency $\omega = \omega_0 - \mathrm{i}\gamma$, in which the real part $\omega_0$ is resonance frequency and the imaginary part $\gamma$ represents the leakage rate. An

* Authors to whom any correspondence should be addressed.

 

exception involves this special Fano resonance of a layer of photonic crystal (PhC) slab, in terms of BICs, which is found residing inside the continuum with zero leakage and infinite lifetimes ($\gamma = 0$, and Q-factor $Q = \omega_0/2\gamma$). The periodic structure (in $x$ and $y$) can support a BIC (in $z$ direction) as a result that the symmetry of the modes determined by this structure mismatching and completely decoupling from the radiating waves. The physical mechanisms of BICs are abundant in different material systems and waves. In this paper, we introduce a novel highly tunable BICs nanostructure consisting of one transverse nanohole and two identical vertical nanoholes (TN-VNs) in one lattice. Our approach provides new insights into the spectral feature of the spectral line shape. We describe two types of BICs of a periodic structure with three nanoholes in one lattice. One type is the at-$\Gamma$ BICs protected by symmetry [9], under a normal incident wave, and the other type is the off-$\Gamma$ BICs achieved through parameter tuning (with coupled resonances or with a single resonance) [10] leading by an oblique incidence.

In this paper, we investigate the BICs of the all-dielectric nanoholes array with ultra-high quality resonances. We study a nanostructure composed of TN-VNs in one lattice, which supports both symmetry-protected and accidental BICs (at-$\Gamma$ and off-$\Gamma$ BICs). Based on the destructive interference between the surface states from the TN element and the identical VNs element, two at-$\Gamma$ BICs emerges, and they can be modulated from modes with infinite Q-factor to Fano modes with finite Q-factor by rotating the electric field polarization direction of the incident plane wave from $x$ to $y$. The off-$\Gamma$ BICs come from the destructive interference from different radiation channels, which can be affected by the in-plane structural parameters insignificantly. Two at-$\Gamma$ BICs and one off-$\Gamma$ BIC of the nanostructure with three nanoholes all have ultra-high Q-factors (more than $10^6$, $10^4$, and $10^6$), which means much in the application of biosensors. Especially, this nanostructure has outstanding ultra-slow light properties at BICs, which underpin a new generation of flat-optics slow light devices.

## 2. Design of structure of the BICs

To demonstrate the BICs phenomenon based on $Si_3N_4$ with refractive index $n_1 = 2.02$, we consider a two-dimensional PhC slab perforated with nanohole arrays (figure 1(a)). The simplest configuration of the unit cell is a nanohole trimer arranged in a square lattice, as shown in figure 1(b). It is composed of TN lying along the $x$ direction and VNs lying along the $y$ direction in a lattice. All notations and parameters related to the geometry of the nanohole array under study are summarized in figure 1. The PhC slab with a thickness of $H = 0.18$ $\mu$m is immersed in a surrounding medium with a refractive index $n_2 = 1.46$.

We excite a model with a p-polarization incident plane wave polarized in $x$ direction propagating from the top and impinging onto the nanostructure in -$z$ direction. For the trimer nanohole array under study, we can recognize the BIC modes by using S4 [30]. Additionally, the temporal coupled mode theory model (CMT) [31, 32] that accounts for the presence of guided leaky resonance in the $Si_3N_4$ layer is also used to demonstrate the study in order to gain deeper physics insight into the resonances.

The reflectance properties of the nanostructure with three nanoholes in one lattice can be simulated by CMT. In one lattice, TN and VNs are two elements exciting two equivalent theoretical coupled modes set as $B$ and $D$. The incoming and outgoing waves in the system are marked by superscripts in and out. The subscript $\pm$ represents two wave propagating directions, as shown in figure 1(c). Therefore, we can get the complex amplitude for the harmonic time dependence of the $n$th mode ($n$ = 1, 2, representing the surface dark modes of each element, respectively) from the coupled equations as follows:

$$\begin{pmatrix} \gamma_1 & -\mathrm{i}\mu_{12} \\ -\mathrm{i}\mu_{21} & \gamma_2 \end{pmatrix} \cdot \begin{pmatrix} a_1 \\ a_2 \end{pmatrix} = \begin{pmatrix} -\tau_{e1}^{-1/2} & 0 \\ 0 & -\tau_{e2}^{-1/2} \end{pmatrix} \cdot \begin{pmatrix} B_+^{in} + B_-^{in} \\ D_+^{in} + D_-^{in} \end{pmatrix} \tag{1}$$

where $\gamma_n = (\mathrm{i}\omega - \mathrm{i}\omega_n - \tau_{in}^{-1} - \tau_{en}^{-1})$, $(n = 1,\ 2)$, $\omega_n\,(n = 1,2)$ is the resonance angular frequency of the $n$th resonator mode, and $\mu_{12}(\mu_{21})$ is the coupling coefficient between them. $1/\tau_{in} = \gamma_{in} = \omega_n/(2Q_{en})$ and $1/\tau_{en} = \gamma_{en} = \omega_n(2Q_{en})$ are the decay rates associated with intrinsic loss and energy escaping into outside space from the resonators ($n$ = 1, 2). $Q_{in}$ and $Q_{en}$ are Q-factors related to the intrinsic loss and the delay rate into outside space in the $n$th resonator, respectively. The relationship between them for the $n$th resonator is $1/Q_{tn} = 1/Q_{in} + 1/Q_{en}$, where $Q_{tn}$ is the total Q-factor of the $n$th resonator. According to the conservation of energy, the equivalent theoretical coupled modes can be given as follows:

$$D_+^{in} = B_+^{out}\mathrm{e}^{\mathrm{i}\varphi}, \quad B_-^{in} = D_-^{out}\mathrm{e}^{\mathrm{i}\varphi} \tag{2}$$

$$B_\pm^{out} = B_\pm^{in} - \tau_{e1}^{-1/2}a_1, \quad D_\pm^{out} = D_\pm^{in} - \tau_{e2}^{-1/2}a_2 \tag{3}$$

where $\varphi = \mathrm{Re}(\beta)d$ represents the total phase difference ($d$ is the effective coupling length between the surface modes).

On the basis of equations (2) and (3) and only one incident wave ($D_-^{in} = 0$), the coefficient $r$ of this system:

$$r = \frac{B_-^{out}}{B_+^{in}} = (\tau_{e1}^{-1}\gamma_2 + \tau_{e2}^{-1}\mathrm{e}^{2\mathrm{i}\varphi}\gamma_1 + (\tau_{e1}\tau_{e2})^{-1/2}\mathrm{e}^{\mathrm{i}\varphi}\chi_1 + (\tau_{e1}\tau_{e2})^{-1/2}\mathrm{e}^{\mathrm{i}\varphi}\chi_2)(\gamma_1\gamma_2 - \chi_1\chi_2)^{-1} \tag{4}$$

where $\chi_1 = \tau_{e1}\tau_{e2})^{-1/2}\mathrm{e}^{\mathrm{i}\varphi} + \mathrm{i}\mu_{12}, \chi_1 = \tau_{e2}\tau_{e1})^{-1/2}\mathrm{e}^{\mathrm{i}\varphi} + \mathrm{i}\mu_{21}$. Hence, reflectance can be obtained as:

$$R = |r|^2. \tag{5}$$

The BIC modes can be distinguished from the other ones by their real-valued eigenfrequencies. We consider the BIC modes in the visible and near-infrared part of the spectrum (0.5 $\mu$m–0.9 $\mu$m). From the known set of modes, we select several BIC modes, which appear in the chosen frequency band for the given parameters of the structure.

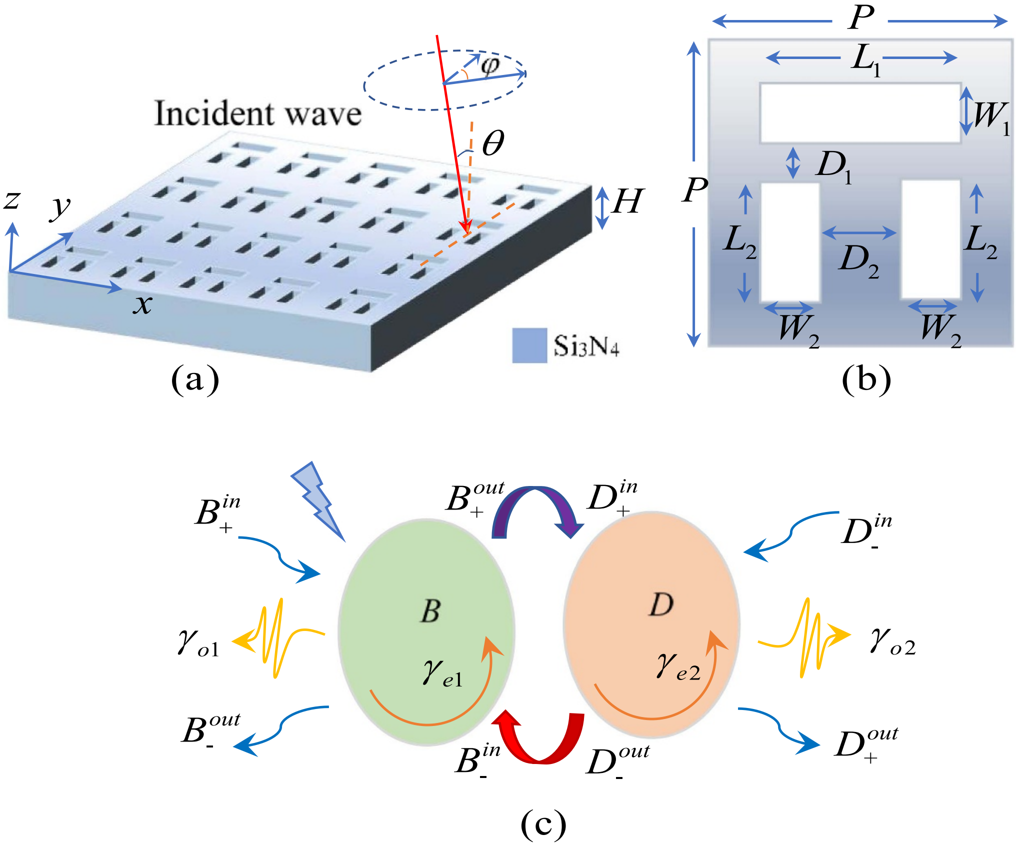


**Figure 1.** (a) Schematic of the periodic 3D structure view of the all-dielectric nanohole array. (b) Top view of a lattice of the periodic structure, and the parameters of this designed structure are as follows: $P = 0.336$ $\mu$m, $L_1 = 0.2$ $\mu$m, $W_1 = 0.06$ $\mu$m, $L_2 = 0.12$ $\mu$m, $W_2 = 0.06$ $\mu$m, $D_1 = 0.036$ $\mu$m, $D_2 = 0.05$ $\mu$m, $H = 0.18$ $\mu$m. (c) The theoretical model of an imaginary resonator, where $B$ and $D$ represent two resonant modes in the CMT.

## 3. Results and discussion

It is known that guided resonance would be excited and sharp Fano features formed in the reflectance spectrum when a plane wave illuminates on the PhC slab [33]. For a symmetry system, the at-Γ modes completely decouple from the far-field radiation as a result of symmetry incompatibility. The incident plane wave is the only radiating states in the normal direction ($z$ direction) which has different symmetry distributions from the surface band states of the structure [1]. Therefore, the Fano resonance peak narrows to zero, the Fano resonance with a zero width here is the at-Γ BIC, and it would be leaky modes if the symmetry protection is broken.

In order to understand the origin of the BICs in a structure composing three nanoholes in one lattice, we consider the uncoupled objects with only TN, only VNs, and TN-VNs in one lattice, respectively. Figure 2 are reflectance for the periodic structure in one lattice with (a) only TN, (b) only VNs, and (c) TN-VNs, respectively. Single at-Γ BIC is observed in figure 2(a) locates at 0.5758 $\mu$m and figure 2(b) that locates at 0.5759 $\mu$m for the structure with only TN and only VNs in one lattice.

When we combine TN and VNs into one lattice, two at-Γ BIC states at 0.5551 $\mu$m, 0.5693 $\mu$m can be obtained obviously in the considered wavelength range (as shown in figure 2(c)). These phenomena mean when the elements of TN and VNs are combined into one lattice, with a separation smaller than the illumination wavelength, their resonant modes interact and form into two new hybridized modes. These hybridized modes are referred to as superradiant mode (bright mode) and a subradiant mode (dark mode) in terms of molecular orbital theory. The bright mode exhibits in-phase oscillations of both dipolar modes, resulting in a large total dipole moment which makes the mode highly radiative. On the contrary, the dark mode has only a small total dipole moment due to the out-of-phase alignment of the dipoles and is a subradiant mode [34].

In the coupled system under study, when the single-nanohole array and the two identical nanohole arrays have different resonances, there are some regions of the spectrum where their phases are matched, forming a bright mode with higher radiance because of constructive interference. On the other hand, in the spectral region where they are out-of-phase, because of destructive interference, two low radiant or subradiant modes are formed (dark modes). The Fano resonance results from the interference of these adiabatic modes that overlap both spectrally and spatially [34].

The dark modes, whose position is determined by a maximum in the reflectance spectrum, are then mainly supported by the three nanoholes and a weak interaction between them. Especially, the two BIC modes of the structure with

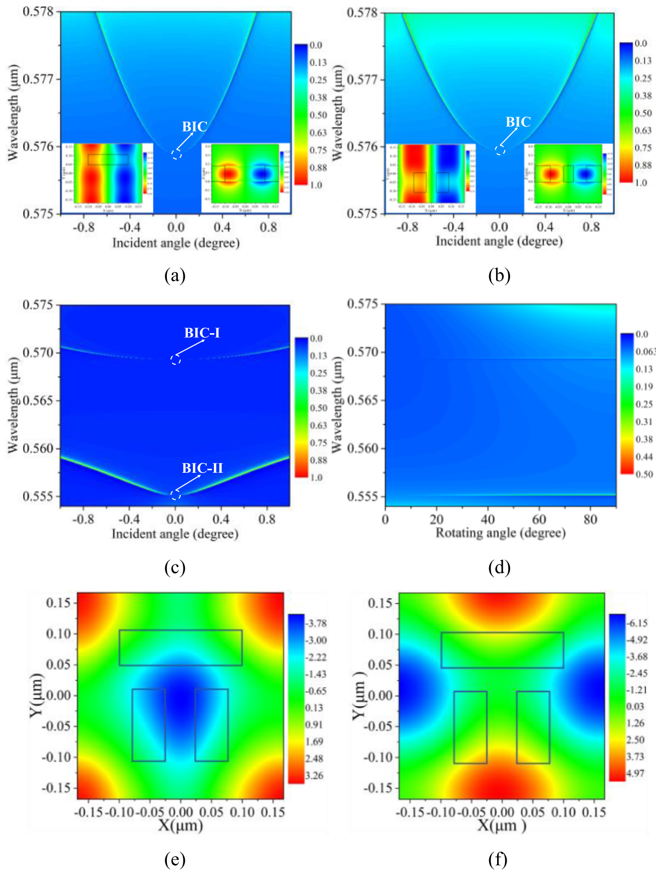


**Figure 2.** Reflectance spectra of the periodic structure in one lattice for (a) TN (the inset shows ***Ez*** component of the near filed distributions of an incident angle near the BICs modes), (b) VNs (the inset shows ***Ez*** component of the near filed distributions of an incident angle near the BICs modes), (c) TN-VNs, and (d) with the polarization direction rotating from $x$ to $y$ for the TN-VNs structure, at incident angle $\theta = 0$ degree. The ***Ez*** components of the near-field distribution at $\theta = 0.01$ degree near the two BICs modes at (e) $\lambda = 0.5551$ $\mu$m and (f) $\lambda = 0.5693$ $\mu$m of the TN-VNs structure.

three nanoholes in one lattice can be influenced by the electric field polarization direction of the incident plane wave. As is shown in figure 2(d), with the electric field polarization direction rotating from $x$ to $y$, the resonance line reappears with a linewidth wider gradually, which means the BIC modes at normal incidence turn into Fano resonances with losses with electric field polarization direction from $x$ rotating away to $y$ ($\varphi = 0$ degree to $\varphi = 90$ degree). As a result, we can adjust the two at-$\Gamma$ BICs by rotating the incident plane wave (electric field polarization) or the direction of the structure symmetry line.

In order to clarify the mechanism of the BIC modes at the $\Gamma$ points, the near-field distribution of the $\boldsymbol{E}_z$ component of the incident angle is plotted near the BICs modes at the x-y cross-section. The insets in figure 2(a) show the near-field distribution $\boldsymbol{E}_z$ components of the incident angle near the BICs mode at the $x$–$y$ cross section at $z = 0$ $\mu$m and at the $x$–$z$ cross section at $y = 0.078$ $\mu$m, respectively. The insets in figure 2(b) show the ***Ez*** components of the near-field distribution of the incident angle near the BICs mode for the $x$–$y$ cross section at $z = 0$ $\mu$m and the $x$–$z$ cross section at $y = -0.048$ $\mu$m, respectively. A slight deviation from the normal incidence introduces a phase shift at the surface of the structure and excites the modes. It can be found that the ***Ez*** dipole is symmetrically distributed around the $x$-direction in the $x$–$y$ cross section and around the $x$–$z$ plane in the $z$-direction. The insets in figures 2(e) and (f) show the near-field distribution of the ***Ez*** component of the incident angle near the BICs mode in the $x$–$y$ cross section at $z = 0$ $\mu$m, respectively. It can be seen from figures 2(e) and (f) that the ***Ez*** dipole is symmetrically distributed in the $x$–$y$ cross section in the $x$ direction in both at-$\Gamma$ BIC modes, and the $x$–$y$ cross section shows a quadrupole associated with the hybridization effect.

The resonant reflectance spectra for the nanostructure are also simulated at a little deflection from normal incidence, as shown in figures 3(a) and (b), by using simulation and theory, respectively, and the results agree well. Figure 3(a) plots the reflectance spectra at an incident angle a small value departure from normal incidence ($\theta = 0.5$ degree), for the structure with only TN (the solid red line) and only VNs (the solid blue line) respectively, while they support independent dipolar resonances with narrow linewidths. For the structure with TN-VNs in one lattice, two hybridized Fano resonance modes come out and they redshift accompanied by the linewidth narrowing with the incident angle approaching zero degree (as shown in figure 3(b)). When the incident angle approaches to

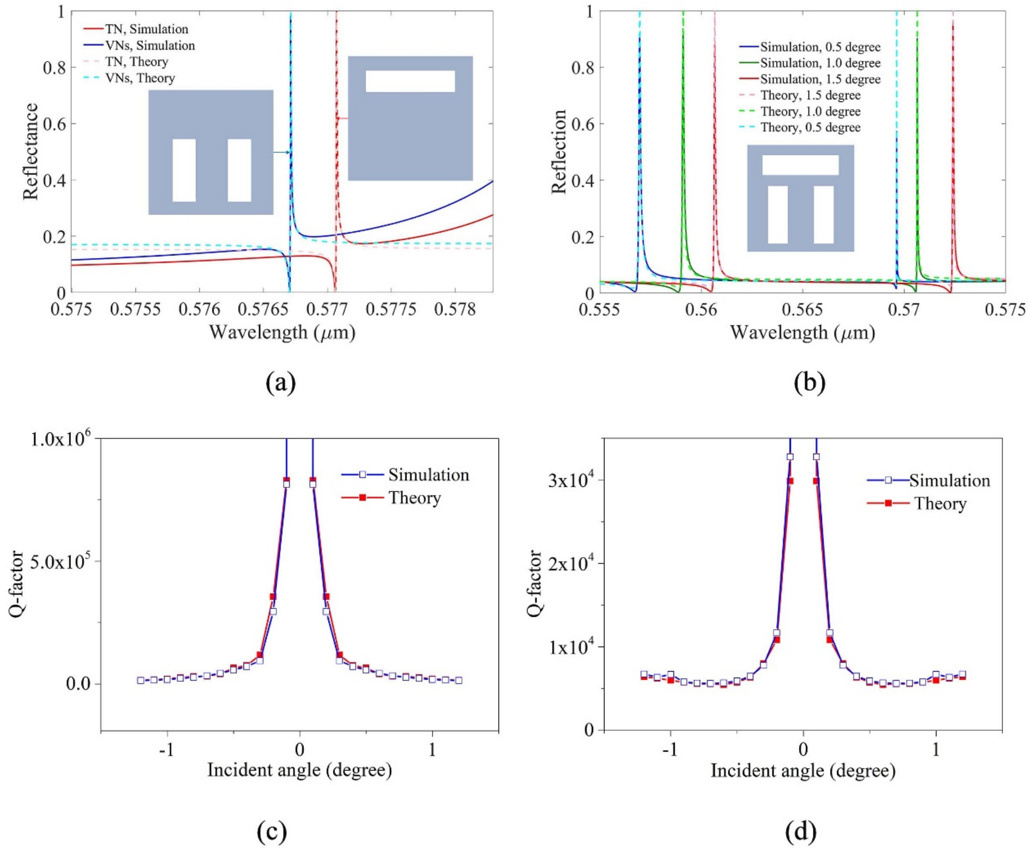


**Figure 3.** Reflectance spectra by both simulation and theory, (a) at incident angle $\theta = 0.5$ degree of the structure with only TN and only VNs in one lattice respectively, (b) at incident angle $\theta = 0.5$ degree, $\theta = 1.0$ degree, $\theta = 1.5$ degree of the structure with TN-VNs in one lattice. Q-factors (c) around BIC-I at about $\lambda = 0.5551$ $\mu$m, (d) around BIC- II at about $\lambda = 0.5693$ $\mu$m of the structure with TN-VNs in one lattice from simulation and theory.

zero, the two dark modes completely decouple from the continuum of free space mode by their symmetry incompatibility, which means the width of Fano resonant modes gets zero at normal incidence, that enables their lifetime approach to infinity. Therefore, more BICs can be obtained by combining TN array and VNs arrays. As a result, we can control the number of the BICs at normal incidence by tuning the structural parameters, which is helpful in the design of novel ultra-high Q-factor sensors. Additionally, we depict the calculated Q-factor of the structure with TN-VNs in one lattice. It reveals that the Q-factor approaches infinite of the structure in figures 3(c) and (d). The Q-factor at the BICs of the structure with three nanoholes in one lattice can exceed $10^6$ at incident angle 0 degree in figure 3(c) at $\lambda = 0.5551$ $\mu$m. Figure 3(d) shows the Q-factor at $\lambda = 0.5693$ $\mu$m around 0 degree is a little lower than that in figure 3(c) but high enough (about $10^4$), and Q-factors of the nanohole structure accord well from both methods. The ultra-high Q-factors of the structures at-$\Gamma$ points are meaningful in many novel potential optical applications.

In an oblique incidence, the reflectance spectrum width disappears at a non-zero angle of 24 degree, 25 degree, and 22 degree, for TN array, VNs array, and TN-VNs arrays, as shown in figures 4(a)–(c), respectively. It is proved that light can be perfectly confined in a periodic nanostructure, and the radiation amplitudes vanish simultaneously as a result of destructive interference [10], which is also a type of BICs always happening at a non-zero incidence angle, and it is associated with the radiation of the constituting waves canceling each other.

Different from two BICs in two reflectance resonant lines in figure 2(c), in figure 4(c), we can see only one resonance line with an off-$\Gamma$ BIC for the periodic three-nanohole structure composed by TN-VNs in a lattice, off-$\Gamma$ BIC are robust to small variation of the structure in-plane parameters, and it is not sensitive to the change of the symmetry or shape of the nanoholes in the structure [1]. For the off-$\Gamma$ BIC mode, when rotating the electric field polarization direction of the incident plane wave from x to y. The BIC mode at incident angle $\theta = 22$ degree, similar to that at incident angle $\theta = 0$ degree, it comes into a Fano resonance with finite Q-factor, which means that off-$\Gamma$ BIC is also influenced by the electric field polarization direction of the incident plane wave (as shown in figure 4(d)). Additionally, the reflectance spectra behave symmetrically about the rotational angle $\varphi = 45$ degree.

In order to clarify the mechanism of the BIC modes at the off $\Gamma$ points, the near-field distribution $\boldsymbol{Ez}$ components of

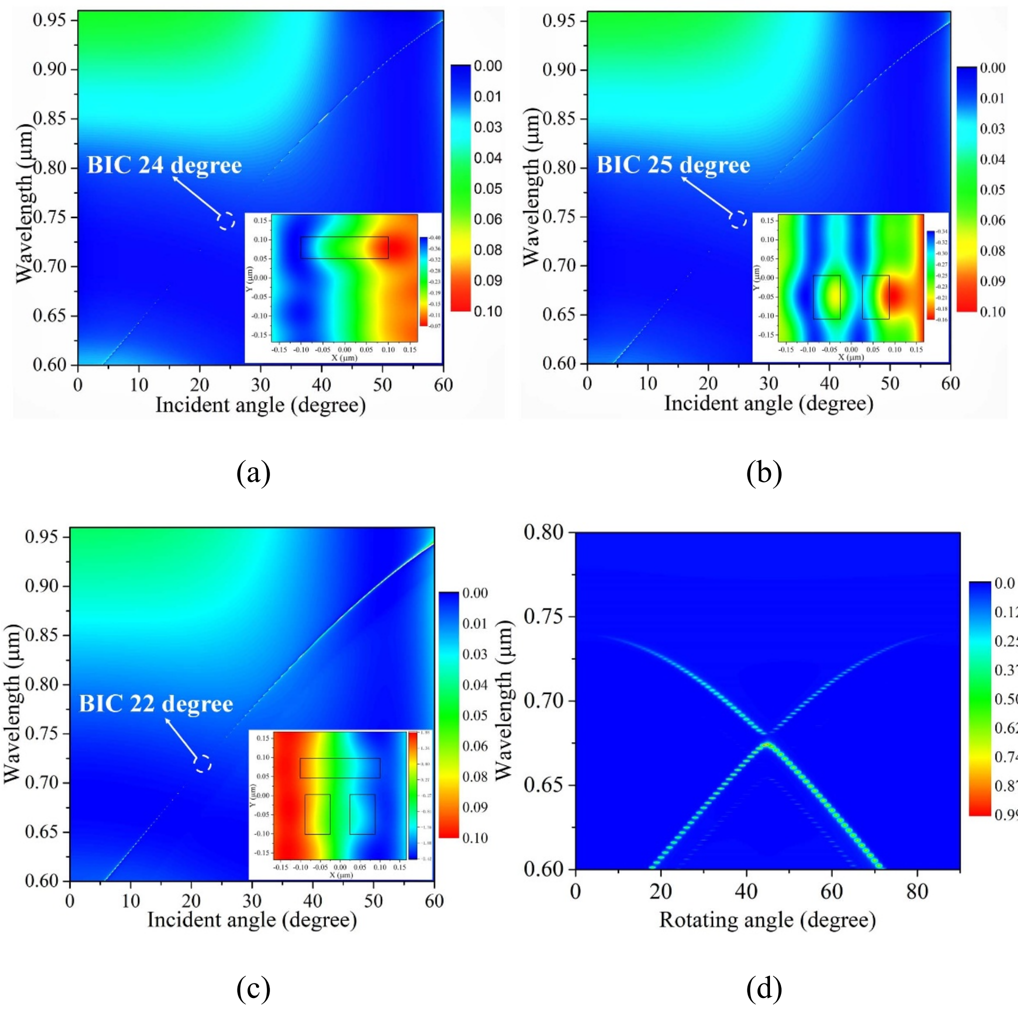


**Figure 4.** Reflectance spectra of the periodic structure in one lattice with (a) TN, (b) VNs, (c) TN-VNs, and (d) the electric field polarization direction rotating from $x$ to $y$ for the periodic structure with TN-VNs in one lattice, at incident angle $\theta = 22$ degree. The inset shows $\boldsymbol{E}_z$ component of the near filed distributions of incident angle (a) $\theta = 24.01$ degree, (b) $\theta = 24.9$ degree, (c) $\theta = 22.01$ degree.

the incident angle are plotted near the BICs mode of the x-y cross-section at $z = 0$ $\mu$m, as shown in figures 4(a)–(c), respectively. The comparison between the three structure cases in the figure shows that the off-Γ BIC are transmitted wave interfering and canceling from different channels [35].

In order to clarify the law of transformation of the off-Γ BIC, we plot the reflectance spectra at 10 degree, 20 degree, and 40 degree of the quasi-BIC peaks of the TN-VNs structure, respectively, and the results from the simulation agree very well with that by theory, as shown in figures 5(a)–(c). It is obvious that the linewidth almost narrows to zero with incident angle approaches to the value ($\theta = 22$ degree) where off-Γ BIC happens. Additionally, we depict the calculated Q-factor of the TN-VNs in figure 5(d). We can observe the Q-factor at an incident angle of $\theta = 22$ degree is of an ultra-high value more than $10^6$. Q-factors of the nanohole structure accord well from both methods. The ultra-high Q-factors of the structures are meaningful in many novel potential optical applications.

The BICs modes with infinite Q-factors are ultra-high sensitive to the change of the nearby or surrounding dielectric medium. The figure of merit ($FOM$) is used for evaluating the performance of a refractive index sensor [36]:

$$FOM = \frac{\Delta f/\Delta n\,(\mathrm{THz/RIU})}{FWHM\,(\mathrm{THz})}. \tag{6}$$

Figure 6(a) shows the FOM of the nanostructure with three nanoholes in one lattice. Where FWHM is the full width at half maximum of the resonant frequency. The corresponding FOM is about $10^4$ RIU$^{-1}$ around the at-Γ BICs and more than $10^5$ RIU$^{-1}$around the off-Γ BIC, which means this nanostructure can have an ultra-high sensibility, much higher than those plasmonic structures [37, 38]. This type of nanostructure with ultra-high FOM to the dielectric environment is of important potential applications such as sensors. Particularly, we can

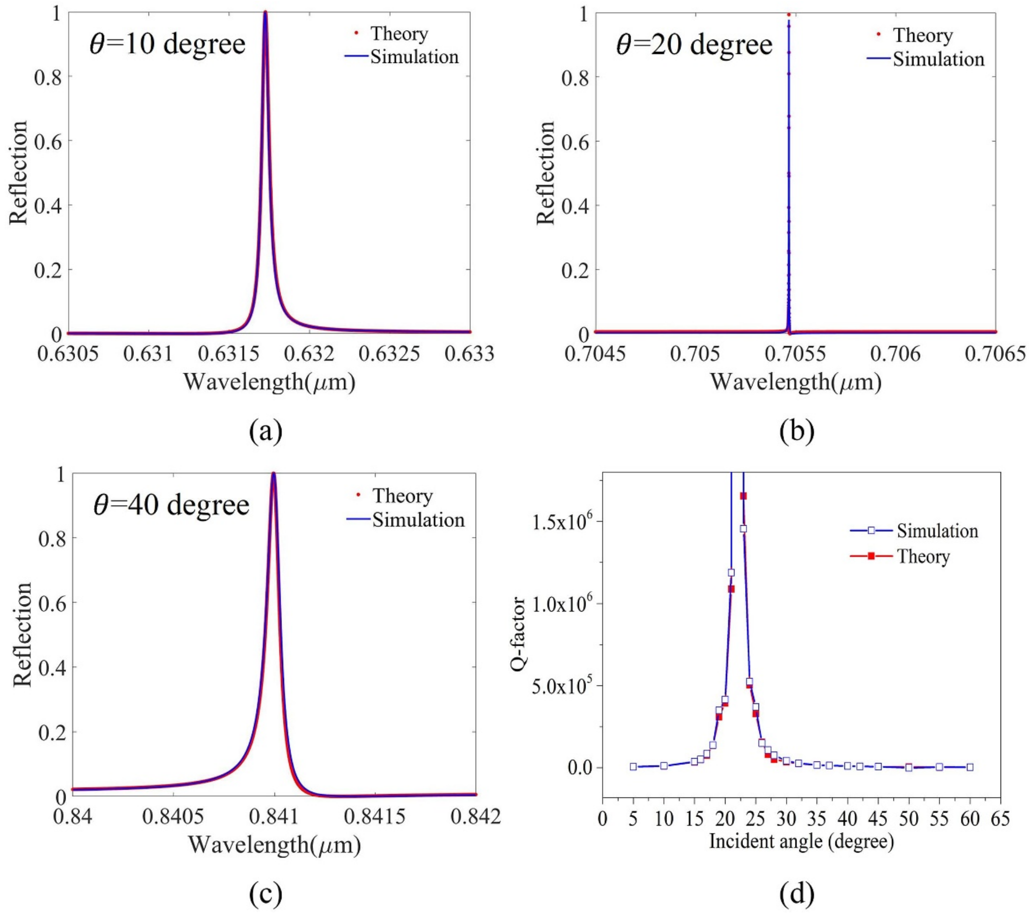


**Figure 5.** Reflectance spectra at incident angle (a) $\theta = 10$ degree, (b) $\theta = 20$ degree, and (c) $\theta = 40$ degree of the structure with TN-VNs in one lattice from simulation and theory. Q-factor (d) around $\theta = 22$ degree for the wavelength reflectance peak at about $\lambda = 0.7199$ $\mu$m of the structure with TN-VNs in one lattice from simulation and theory.

control the number of the BIC modes of this kind of sensor by modulating the structural parameters.

From the previous analysis, in case the incident angle is around zero, we can treat the structure TN and VNs act as two elements forming dark modes, which interact between the elements and create an electromagnetically induced transparency like phenomenon with two new dark modes (subradiant modes) and one wide bright mode (superradiant mode) between the two modes. At normal incidence, as a result of symmetry incompatibility, the two dark modes change into at-$\Gamma$ BICs. At an oblique incidence, an off-$\Gamma$ BIC is also found at about 22 degree as a result of the canceling interference between different channels, which is affected insignificantly by the in-plane structural parameters.

The surface modes of the nanostructure with TN-VNs in the system produce interactions around the resonant positions, leading to dispersion. The dispersion effect can be used to realize the slow light application. Group index has a positive correlation with the slow light effect, we can use it to value the slow light devices [39]. The group index can be expressed as equation (7):

$$n_g = \frac{c}{H}\frac{\mathrm{d}\eta}{\mathrm{d}\omega} \tag{7}$$

where c is the speed of light in vacuum, $H = 0.18$ $\mu$m denotes the thickness of the metasurface. $\eta = \arg(\mathrm{r})$ can be obtained from the reflectance coefficient calculated by equation (4) indicating the reflectance phase.

Because the zero line width at the BICs, we take the quasi-BICs resonance line to investigate the slow light effect. The group index and phase shift of the metasurface are shown in figures 6(c) and (d). It is clear that two ultra-high values of the group index appear for the two dark modes located at 0.5569 $\mu$m and 0.5696 $\mu$m at an incidence angle of $\theta = 0.5$ degree. There is also an ultra-high value of the group index at 0.7055 $\mu$m with $\theta = 20$ degree. The quasi at-$\Gamma$ BIC mode and the quasi off-$\Gamma$ BIC mode reach positive values over $10^5$, which indicates a slow light effect. Meanwhile, the phase fluctuates as a result of the interaction at the resonant wavelength, they all transform from high values to low values. The slow light effect is more significant than that of the

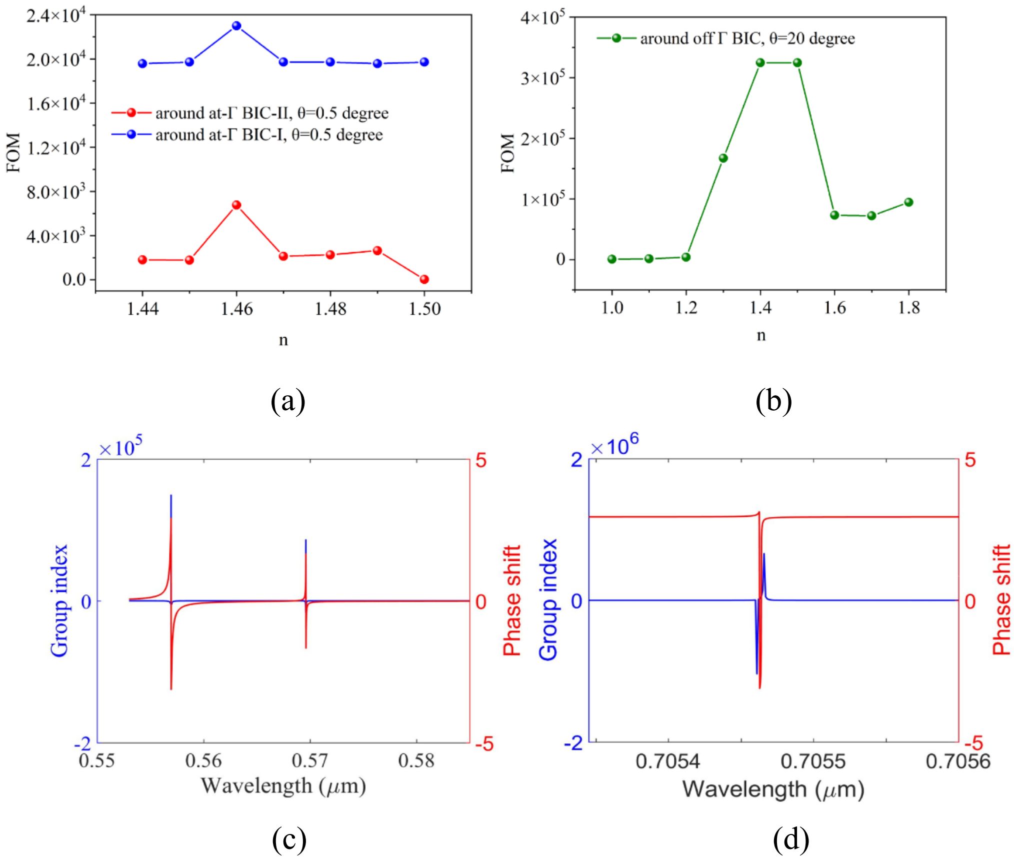


**Figure 6.** FOM versus the refractive index of the surrounding medium of the structure with TN-VNs in one lattice at the incident angle (a) $\theta = 0.5$ degree and (b) $\theta = 20$ degree, respectively. Group refractive index and phase shift versus wavelength of the structure with TN-VNs in one lattice at the incident angle (c) $\theta = 0.5$ degree and (d) $\theta = 20$ degree, respectively.

plasmonic waveguide device. It proposes a new approach to designing ultra-slow light devices.

## 4. Conclusions

In conclusion, an integral nanohole array perforated in a layer of $Si_3N_4$ PhC slab surrounded by silica medium is numerically and theoretically analyzed by S4 and CMT, respectively. For the at-Γ BICs, TN array and VNs array have BICs at different wavelengths. When we compact the two types of nanoholes as two elements into one lattice, the surface modes in different spectra would interfere destructively and two new surface modes appear, and they form into BICs at the Γ points. The off-Γ BICs can be affected insignificantly by the in-plane structure parameters. Both at-Γ BICs of the three-nanohole nanostructure exhibit high tunability by the polarization direction of the incident plane wave. Q-factors of two at-Γ BICs and one off-Γ BIC can exceed $10^6$, $10^4$, and $10^6$, respectively. The slow light property of the nanohole structure at the BICs is also explored, and ultra-slow light is obtained with the group index exceeding $10^6$. The proposed design is essential for understanding the fundamental mechanism of the BICs and the tuning of multiple BICs. The results could promote practical applications of all-dielectric devices, including efficient biosensing, perfect filters, a detector for impurities within a structure, and ultra-slow light devices.

## Data availability statement

The data that support the findings of this study are available upon reasonable request from the authors.

## Acknowledgments

This work was supported by Natural Science Foundation of China (Grant Nos. 11304094, 62027810 and 12172228), Hunan Provincial National Natural Science Foundation of China (Grant No. 2020JJ5153), and Natural Science Foundation of Shanghai (Grant No.22ZR1444400).

## ORCID iD

Suxia Xie https://orcid.org/0000-0003-2499-5914

## References

[1] Huang L, Xu L, Powell D A, Padilla W J and Miroshnichenko A E 2023 Resonant leaky modes in all-dielectric metasystems: fundamentals and applications *Phys. Rep.* **1008** 1–66
[2] Liu T, Qin M, Wu F and Xiao S 2023 High-efficiency optical frequency mixing in an all-dielectric metasurface enabled

by multiple bound states in the continuum *Phys. Rev.* B **107** 075441

[3] Xiao S, Qin M, Duan J, Wu F and Liu T 2022 Polarization-controlled dynamically switchable high-harmonic generation from all-dielectric metasurfaces governed by dual bound states in the continuum *Phys. Rev.* B **105** 195440

[4] Huang L, Xu L, Woolley M and Miroshnichenko A E 2020 Trends in quantum nanophotonics *Adv. Quantum Technol.* **3** 1900126

[5] Paddon P and Young J F 2000 Two-dimensional vector-coupled-mode theory for textured planar waveguides *Phys. Rev.* B **61** 2090–101

[6] Xu L *et al* 2020 Enhanced light–matter interactions in dielectric nanostructures via machine-learning approach *Adv. Photon.* **2** 026003

[7] Huang L, Xu L, Rahmani M, Neshev D and Miroshnichenko A 2021 Pushing the limit of high-Q mode of a single dielectric nanocavity *Adv. Photon.* **3** 016004

[8] Huang C *et al* 2020 Ultrafast control of vortex microlasers *Science* **367** 1018–21

[9] Yu Y, Sakanas A, Zali A R, Semenova E, Yvind K and Mørk J 2021 Ultra-coherent Fano laser based on a bound state in the continuum *Nat. Photon.* **15** 758–64

[10] Wang J, Zhao M, Liu W, Guan F, Liu X, Shi L, Chan C T and Zi J 2021 Shifting beams at normal incidence via controlling momentum-space geometric phases *Nat. Commun.* **12** 6046

[11] Zheng Z, Zhu Y, Duan J, Qin M, Wu F and Xiao S 2021 Enhancing Goos-Hanchen shift based on magnetic dipole quasi-bound states in the continuum in all-dielectric metasurfaces *Opt. Express* **29** 29541–9

[12] Al-Ani I A M, As'Ham K, Huang L, Miroshnichenko A E and Hattori H T 2021 Enhanced strong coupling of TMDC monolayers by bound state in the continuum *Laser Photon. Rev.* **15** 2100240

[13] Al-Ani I A M, As'Ham K, Huang L, Miroshnichenko A E, Lei W and Hattori H T 2022 Strong coupling of exciton and high-q mode in all-perovskite metasurfaces *Adv. Opt. Mater.* **10** 2101120

[14] Li J, Li J, Zheng C, Yue Z, Yang D, Wang S, Li M, Zhang Y and Yao J 2021 Spectral amplitude modulation and dynamic near-field displaying of all-silicon terahertz metasurfaces supporting bound states in the continuum *Appl. Phys. Lett.* **119** 241105

[15] Hu Y, Tong M, Hu S, He W, Cheng X and Jiang T 2022 Spatiotemporal lineshape tailoring in BIC-mediated reconfigurable metamaterials *Adv. Funct. Mater.* **32** 2203680

[16] Xu L *et al* 2019 Dynamic nonlinear image tuning through magnetic dipole quasi-BIC ultrathin resonators *Adv. Sci.* **6** 1802119

[17] Wang Y, Han Z, Du Y and Qin J 2021 Ultrasensitive terahertz sensing with high-Q toroidal dipole resonance governed by bound states in the continuum in all-dielectric metasurface *Nanophotonics* **10** 1295–307

[18] Gentry C M and Popović M A 2014 Dark state lasers *Opt. Lett.* **39** 4136–9

[19] Ha S T, Fu Y H, Emani N K, Pan Z, Bakker R M, Paniagua-Domínguez R and Kuznetsov A I 2018 Directional lasing in resonant semiconductor nanoantenna arrays *Nat. Nanotechnol.* **13** 1042–7

[20] Kodigala A, Lepetit T, Gu Q, Bahari B, Fainman Y and Kanté B 2017 Lasing action from photonic bound states in continuum *Nature* **541** 196–9

[21] Penzo E, Romano S, Wang Y, Dhuey S, Negro L D, Mocella V and Cabrini S 2017 Patterning of electrically tunable light-emitting photonic structures demonstrating bound states in the continuum *J. Vac. Sci. Technol.* B **35** 06G401

[22] Rybin M and Kivshar Y 2017 Supercavity lasing *Nature* **541** 164–5

[23] Foley J M and Phillips J D 2015 Normal incidence narrowband transmission filtering capabilities using symmetry-protected modes of a subwavelength, dielectric grating *Opt. Lett.* **40** 2637–40

[24] Foley J M, Young S M and Phillips J D 2014 Symmetry-protected mode coupling near normal incidence for narrow-band transmission filtering in a dielectric grating *Phys. Rev.* B **89** 165111

[25] Dong Z *et al* 2022 Schrödinger's red pixel by quasi-bound-statesin-the-continuum *Sci. Adv.* **8** eabm4512

[26] Dong Z *et al* 2022 Nanoscale mapping of optically inaccessible bound-states-in-the-continuum *Light: Sci. Appl.* **11** 20

[27] Romano S, Lamberti A, Masullo M, Penzo E, Cabrini S, Rendina I and Mocella V 2018 Optical biosensors based on photonic crystals supporting bound states in the continuum *Materials* **11** 526

[28] Romano S, Zito G, Torino S, Calafiore G, Penzo E, Coppola G, Cabrini S, Rendina I and Mocella V 2018 Label-free sensing of ultralow-weight molecules with all-dielectric metasurfaces supporting bound states in the continuum *Photon. Res.* **6** 726–33

[29] Carletti L, Koshelev K, De Angelis C and Kivshar Y 2018 Giant nonlinear response at the nanoscale driven by bound states in the continuum *Phys. Rev. Lett.* **121** 033903

[30] Liu V and Fan S 2012 S4: a free electromagnetic solver for layered periodic structures *Comput. Phys. Commun.* **183** 2233–44

[31] Fan S, Suh W and Joannopoulos J D 2003 Temporal coupled-mode theory for the Fano resonance in optical resonators *J. Opt. Soc. Am.* A **20** 569–72

[32] Xu H, Xiong C, Chen Z, Zheng M, Zhao M, Zhang B and Li H 2018 Dynamic plasmon-induced transparency modulator and excellent absorber-based terahertz planar graphene metamaterial *J. Opt. Soc. Am.* B **35** 1463–8

[33] Fan S and Joannopoulos J D 2002 Analysis of guided resonances in photonic crystal slabs *Phys. Rev.* B **65** 235112

[34] Lovera A, Gallinet B, Nordlander P and Martin O J F 2013 Mechanisms of Fano resonances in coupled plasmonic systems *ACS Nano* **7** 4527–36

[35] Xie S, Yang J, Tian G, Shen W and Bai C 2023 Modulation of the multiple bound states in the continuum of the all-dielectric metasurface *Photonics* **10** 418

[36] Sherry L J, Chang S-H, Schatz G C, Van Duyne R P, Wiley B J and Xia Y 2005 Localized surface plasmon resonance spectroscopy of single silver nanocubes *Nano Lett.* **5** 2034–8

[37] Hao F, Sonnefraud Y, Dorpe P V, Maier S A, Halas N J and Nordlander P 2008 Symmetry breaking in plasmonic nanocavities: subradiant LSPR sensing and a tunable Fano resonance *Nano Lett.* **8** 3983–8

[38] Hao F, Nordlander P, Sonnefraud Y, Dorpe P V and Maier S A 2009 Tunability of subradiant dipolar and Fano-type plasmon resonances in metallic ring/disk cavities: implications for nanoscale optical sensing *ACS Nano* **3** 643–52

[39] Liu C, Li H, Xu H, Zhao M, Xiong C, Zhang B and Wu K 2019 Slow light effect based on tunable plasmon-induced transparency of monolayer black phosphorus *J. Phys. D: Appl. Phys.* **52** 405203